MMAE Delivery Using the *Bicycle* Toxin Conjugate BT5528 AC

Gavin Bennett[1], Amy Brown[1], Gemma Mudd[1], Philip Huxley[1], Katerine Van Rietschoten[1], Silvia Pavan[2], Liuhong Chen[1], Sophie Watcham[3], Johanna Lahdenranta[4], and Nicholas Keen[4]

ABSTRACT

The EphA2 receptor is found at high levels in tumors and low levels in normal tissue and high EphA2 expression in biopsies is a predictor of poor outcome in patients. Drug discovery groups have therefore sought to develop EphA2-based therapies using small molecule, peptide, and nanoparticle-based approaches (1–3). However, until now only EphA2-targeting antibody–drug conjugates (ADC) have entered clinical development. For example, MEDI-547 is an EphA2-targeting ADC that displayed encouraging antitumor activity in preclinical models and progressed to phase I clinical testing in man. Here we describe the development of BT5528, a bicyclic peptide ("*Bicycle*") conjugated to the auristatin derivative maleimidocaproyl-monomethyl auristatin E to generate the *Bicycle* toxin conjugate BT5528. The report compares and contrasts the Pharmacokinetics (PK) characteristics of antibody and *Bicycle*-based targeting systems and discusses how the PK and payload characteristics of different delivery systems impact the efficacy—toxicity trade off which is key to the development of successful cancer therapies. We show that BT5528 gives rise to rapid update into tumors and fast renal elimination followed by persistent toxin levels in tumors without prolonged exposure of parent drug in the vasculature. This fast in, fast out kinetics gave rise to more favorable toxicology findings in rats and monkeys than were observed with MEDI-547 in preclinical and clinical studies.

Graphical Abstract: http://mct.aacrjournals.org/content/molcanther/19/7/1385/F1.large.jpg.

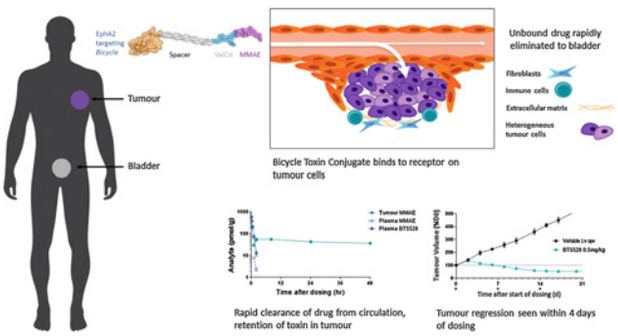

Introduction

The goal of cancer therapy is to selectively kill cancer cells while sparing normal cells. First-generation cancer therapies achieved this by targeting rapidly dividing cancer cells with cytotoxic agents. Although this approach achieved some success, the mechanism—inhibition of cell division—was conceptually flawed since, while tumor cells proliferate rapidly, so do those required for normal physiology—particularly those in the gastrointestinal (GI) tract and bone marrow. The utility of cytotoxic drugs is therefore limited by their poor therapeutic index.

In principle, selective delivery of cytotoxic drugs to tumor cells should improve efficacy and decrease side effects on nontarget organs. This desire for selective tumor targeting led to the development of antibody–drug conjugates (ADC), in which the cytotoxin is attached to an antibody that recognizes an extracellular antigen that is overexpressed by tumor cells and has lower or absent expression in normal tissue. This paradigm first achieved clinical success with the ADC Mylotarg, a CD33 mAb linked to a calicheamicin cytotoxic and approved for the treatment of relapsed acute myelogenous leukemia in 2000 (4–6). Despite the clinical success of several ADCs, antibodies did not evolve to deliver payloads to tumors, and have intrinsic limitations in this application. First, they are sufficiently large (ca.150 kDa) that they poorly extravasate and are ineffective in delivering their payload to poorly perfused tumor tissue (7, 8). Second, ADCs are characterized by long *in vivo* half-lives and plateau-like PK profiles. This PK profile can give rise to toxin release and toxicity in nontarget organs, which express the target antigen at low levels. Finally, antibodies are characteristically eliminated via hepatic metabolism, leading to release of payload in the liver and GI tract—hepatic and GI toxicities are therefore common dose-limiting toxicities for ADCs (9). Therefore, a different approach to targeting cytotoxins to tumors without these inherent disadvantages is merited.

In this publication, we describe such a distinct approach, in which the mAb is replaced with a synthetic, structurally constrained bicyclic peptide ("*Bicycle*") targeting the erythropoietin-producing hepatocellular (Eph) receptor, EphA2, to generate a *Bicycle* toxin conjugate (BTC).

The Erythropoietin-producing hepatocellular (Eph) receptors comprise a large family of receptor tyrosine kinases that are activated in response to binding by Eph receptor-interacting proteins (Ephrins). Ephs form the largest known subfamily of receptor tyrosine kinases (RTK). The EphA2 receptor plays a role in development (10), but is expressed at relatively low levels in normal adult tissue (11, 12).

[1]Bicycle Therapeutics, Cambridge, United Kingdom. [2]Fabbrica Italiana Sintetici S.p.A., Vicenza, Italy. [3]Isogenica, Cambridge, United Kingdom. [4]Bicycle Therapeutics, Lexington, Massachusetts.

Note: Supplementary data for this article are available at Molecular Cancer Therapeutics Online (http://mct.aacrjournals.org/).

Corresponding Author: Gavin Bennett, Bicycle Therapeutics, Building B900, Babraham Research Campus, Cambridge, Cambridgeshire cb223at, UK. Phone: 441223261503; E-mail: gavin.bennett@bicycletx.com

Mol Cancer Ther 2020;19:1385–94

doi: 10.1158/1535-7163.MCT-19-1092

Overexpression has been reported across a wide range of solid tumors including ovarian, endometrial, and cervical cancers, melanoma, and gliomas (13–24), and is associated with poor patient outcome (25–28), making it an ideal target for EphA2 selective payload targeting using ADCs and other approaches. For example, MEDI-547 is an ADC comprising an EphA2 targeted mAb (1C1) conjugated to the auristatin derivative maleimidocaproyl-monomethyl auristatin phenylalanine (mcMMAF). MEDI-547 displayed encouraging antitumor activity in preclinical models (18, 29) and was progressed to clinical evaluation in a phase I study. However, the study was halted following treatment-related bleeding and coagulation events, and liver enzyme elevations at the starting dose and there are no plans to continue clinical development (30). These clinical findings were consistent with preclinical findings in rats and monkeys, where increased activated partial thromboplastin time, increased fibrinogen/fibrin degradation product, and fibrin D dimer and bleeding events were reported (30). Preclinical studies in the monkey and clinical testing in humans pointed to disseminated intravascular coagulation (DIC) as the dose-limiting toxicology (30). Continued investigation of EphA2 to target toxin delivery is therefore dependent on evidence that alternative delivery modalities will not give rise to analogous adverse events in patients.

This work demonstrates that BTCs and ADCs have distinct physico-chemical and *in vivo* properties. BTCs are much smaller than ADCs (molecular weight ca.4 kDa vs. ca.150 kDa), with a physicochemical profile characteristic of renally excreted molecules, and have short plasma half-lives measured in minutes not hours. However, this short plasma half-life is balanced by rapid and efficient tumor penetration (resulting from the low molecular weight), a high C_{max}, and release of a cell penetrant payload, giving rise to bystander killing in the tumor microenvironment.

We hypothesized that because the PK profile of BTCs gives rise to much lower cumulative exposure of parent drug to normal tissue than ADCs, BTCs might give rise to a more favorable therapeutic index than MEDI-547. We therefore developed BT5528, a novel BTC targeting EphA2 expressing tumors and embarked on PK, efficacy, and toxicology studies aimed at de-risking the toxicology observed with MEDI-547, and demonstrating that peptide based EphA2 targeting agents merit clinical evaluation in patients.

Materials and Methods

A brief summary of the methods is provided below. Detailed protocols are described in Supplementary Materials and Methods online.

Phage optimization of EphA2 binding peptides

Bicycle binders were selected by phage display using methods described in Heinis (31).

In vitro studies

Binding affinities were determined using a fluorescence polarization competition assay and surface plasmon resonance assays using conventional methods.

Cell binding

Binding of BTCs to cells was assessed by high content screening. Fibrosarcoma HT1080 cells were incubated with BTC for 45 minutes at 4°C, with binding visualized using an anti-MMAE antibody conjugated to fluorescein.

Endogenous EphA2 expression on human cell lines

EphA2 expression in tumor cells or patient-derived tumor samples was quantified by measurement of EphA2 antibody binding using flow cytometry. Absolute antibody binding sites on cells were also quantified (using QuantiBRITE beads; BD Biosciences).

Plasma protein binding, stability in plasma and hepatocytes

Plasma protein binding and stability was assessed in CD1 mouse, Sprague–Dawley rat, Cynomolgus monkey, and human plasma. Stability was also assessed in human hepatocytes. Studies were conducted at Wuxi AppTec Co. Ltd. using conventional protocols.

Quantifying BT5528 and MMAE in plasma and tumor

BT5528 and MMAE levels were quantified in plasma and tumor samples following analyte extraction and bioanalysis using LC/MS-MS assays.

Measurement of pHH3 in tumor samples

Tumor samples were fixed, embedded in paraffin, stained for pHH3 and pHH3 positive nuclei were quantified using image analysis software.

Xenograft models

Xenograft models were conducted in 6- to 8-week-old female balb/c nude or CB17-SCID mice inoculated with $\sim 10^7$ cells in the right flank. Animals were randomized when the average tumor volume reached the predesignated start size. Group size ranged from $n = 3$ to 6. All studies included a vehicle-treated control. For patient-derived xenograft models a tumor fragment ($\sim$30 mm^3) was used for inoculation. Dosing was conducted by intravenous bolus. Tumor volumes were measured using a caliper, and the volume calculated as V (mm^3) $= 0.5a \times b^2$, where a and b are the long and short diameters of the tumor, respectively. All Xenograft studies were conducted at Wuxi AppTec Co. Ltd.

PET imaging

Imaging studies were conducted at Bioprobe Ltd., using mice bearing subcutaneous HT-1080 xenografts. The labeled binder (BCY6164) was synthesized by conjugating the *Bicycle* binder BCY6099 to a DOTA chelator which was subsequently incubated with Ga-68 chloride to generate radiolabeled test article. Mice were anesthetized and administered BCY6164 intravenously ($\sim$150 pmol, $\sim$1.5–2.5 MBq) as a 200 μL bolus over 15 to 25 seconds. Imaging was performed using PET/CT scanning and images constructed using imaging software.

Toxicology studies

Toxicology studies were conducted at Envigo Ltd., in accordance with the recommendations of ICH S9 Nonclinical Evaluation for Anticancer Pharmaceuticals. Rats and nonhuman primates (NHP, cynomolgus monkeys) were dosed BT5528 once weekly for five doses in a 32-day study. Evaluations included clinical signs, body weight and food consumption, macroscopic and microscopic pathology, hematology, clinical chemistry, urinalysis, coagulation, and toxicokinetics.

Results

Engineering high affinity EphA2 binder and control molecules

Lead EphA2 binders were identified using proprietary phage display technology (31), which allowed us to rapidly identify low nmol/L hits and define robust amino side chain SAR. Lead optimization aimed at

improving stability and increasing hydrophilicity was carried out using standard fmoc solid-phase synthesis guided by x-ray crystallography studies (32). This work gave rise to BCY6099, a hydrophilic *Bicycle* peptide with low nmol/L EphA2 binding and excellent stability in mouse, monkey, and human plasma (Supplementary Information T1 and T3).

Having identified a lead *Bicycle* we focused our chemistry effort on optimizing conjugation chemistry: the molecular spacer, cleavable linker, and toxin payload. In the course of this optimization work, we synthesized >75 BTCs exploring spacer, linker, and payload SAR. The screening cascade comprised binding affinity for human, rat, mouse, and monkey EphA2, selectivity over related Eph receptors, physicochemical and ADME properties, efficacy in xenograft models and toxicology readouts in the rat and monkey. This work culminated in the identification of the lead candidate BT5528.

BT5528, the BT5528 parent *Bicycle* molecule (BCY6099), negative control compounds, and a DOTA analogue used for imaging studies are all fully described in Supplementary Chemical Structures. In this work the EphA2 ADC (denoted 1C1-mcMMAF) was used as a surrogate for MEDI-547.

In vitro binding profile

In vitro binding studies showed that attaching the auristatin toxin payload to BCY6009 has minimal impact on binding affinity (BCY6099: $K_D = 5.7 \pm 0.9$ nmol/L; BT5528: $K_D = 1.9 \pm 0.9$ nmol/L; Supplementary Information T1). We also showed that optimizing affinity to human EphA2 on phage gave rise to binders with high affinity for mouse, rat, and cynomolgus monkey EphA2 (Supplementary Information T1); and furthermore that BT5528 is highly selective (>5,000-fold) for EphA2 over closely related human and rodent homologs (Epha3-7); and Eph family members that play a critical role in proinflammatory signaling (5) (EphB1) and vascular development (33) and bone remodeling (EphB4; Supplementary Information T2; ref. 34).

HCS binding studies

We used high content screening assays to show that BT5528 (but not nonbinding controls) bind to the surface of HT-1080 cells, which express high levels of EphA2 (**Fig. 1A–D**; Supplementary Information T5a). BT5528, the ADC 1C1-mcMMAF, and negative controls, BCY6079 and MMAE, were incubated with HT-1080 cells for 45 minutes at 4°C and binding visualized using an anti-MMAE antibody. **Figure 1A** and **B** show that BT5528 and 1C1-mcMMAF bind on the entire HT1080 cell surface. No staining was observed with cells incubated with MMAE, or BCY6079, a nonbinder negative control (**Fig. 1C** and **D**).

Biodistribution studies

We conducted biodistribution studies with a Ga-68 radiolabeled *Bicycle* binder BCY6064 (BCY6099 conjugated to a DOTA chelating group) using microPET imaging studies. **Figure 1E** shows that BCY6064 exhibits high and specific tumor targeting (max $12 \pm 6.3\%$ ID/g at 30 minutes postdose), low uptake in nontarget tissues, and rapid clearance of excess peptide through the kidney to the bladder. The biodistribution study also confirmed that although the *Bicycle* binder is only transiently present in plasma, it maintains high and persistent levels in tumor tissue (**Fig. 1F**).

In vitro and *in vivo* PK parameters

BT5528 is metabolically stable *in vitro* in rat, cynomolgus, and human plasma and human hepatocytes, with low clearance values (Cl_{int}) in all species (Supplementary Information ST3). BT5528 is less stable in mouse plasma probably because of the presence of the esterase Ces1c, which is known to cleave the valine–citruline peptide linker (35). BT5528 exhibits low plasma protein binding (fu_p 0.32–0.49) in mouse, rat, cynomolgus, and human (Supplementary Information T3).

In vivo pharmacokinetic parameters of BT5528 were determined in mouse, rat, and cynomolgus monkey plasma following intravenous administration at 1 mg/kg. Plasma concentration–time curves and PK parameters provide evidence of similar PK profiles for both rodent and nonrodent species (Supplementary Information S1 and T4). Intact BT5528 demonstrated a peptide-like PK profile across species with short terminal half-lives: 0.4 hours (mouse), 0.3 hours (rat), and 0.6 hours (nonhuman primate) with a low rate of payload release in plasma (Supplementary Information S1 and T4). Free MMAE was also measured in plasma, but observed levels were low and decreased rapidly after dosing (Supplementary Information S1 and T4).

In contrast to the peptide-like PK profile, we observe with BT5528, MEDI-547 exhibited a typical ADC-like profile following dosing to patients (30). Thirty minutes after intravenous administration at 0.08 mg/kg mean MEDI-547 levels were 2.14 μg/mL. Three days after dose parent drug concentrations were still 0.67 μg/mL, implying a terminal half-life in excess of 24 hours. In contrast, plasma concentrations for MMAF metabolites were below the lower limit of detection (0.2 ng/mL) at all time points in all patients (30). These results are as expected for the stable maleimidocaproyl (mc) linker, which was designed to resist extracellular cleavage and release payload following receptor internalization and cleavage in the lysozyme.

The PK results therefore confirm that peptide and antibody toxin delivery systems give rise to profoundly different *in vivo* PK profiles.

Figure 2A–D illustrate results from a PK/PD study in the PC3 xenograft model. PK results in the BT5528 xenograft study are consistent with the BCY6064 biodistribution study described above: transient parent drug and MMAE levels in plasma and plateau like MMAE levels in tumor samples persisting to 48 hours and beyond (**Fig. 2A**). In the same study we observed excellent tumor regression using a low 0.5 mg/kg dose of BT5528 (**Fig. 2B**). MMAE acts as an antimitotic agent, which causes mitotic arrest though inhibition of tubulin polymerization. We used IHC staining for phosphohistone H3 (pHH3) in fixed PC3 tumors to demonstrate the accumulation of mitotic cells during mitotic arrest brought on by MMAE levels in the tumor xenografts. The tumor regression shown in **Fig. 2B** is thus consistent with the progressively increased PHH3 staining (from early time points to the final 48-hour time point) demonstrated in **Fig. 2C** and **D**.

In vivo mechanism of action and efficacy studies

BTCs rely on toxin delivery via linker cleavage and release of a cell penetrant microtubule inhibitor. It is therefore important to show that *in vivo* efficacy is driven by targeted delivery to EphA2 expressing cells, as opposed to nontargeted toxin release in the systemic circulation. We therefore assessed *in vivo* potency in low, medium, and high cell line derived xenograft (CDX) and patient-derived (PDX) models (Supplementary Information T5a and T5b). **Figure 3** illustrates the observed relationship between EphA2 expression and efficacy. It is clear from **Fig. 3** that EphA2 expression is a key determinant of BT5528 efficacy in murine xenograft models. The complete *in vivo* dataset can be found in Supplementary Information S2 and S3.

Further *in vivo* xenograft experiments were designed to increase our understanding of the molecular mechanisms mediating *Bicycle*-based toxin delivery and to compare BTC- and ADC-based toxin delivery.

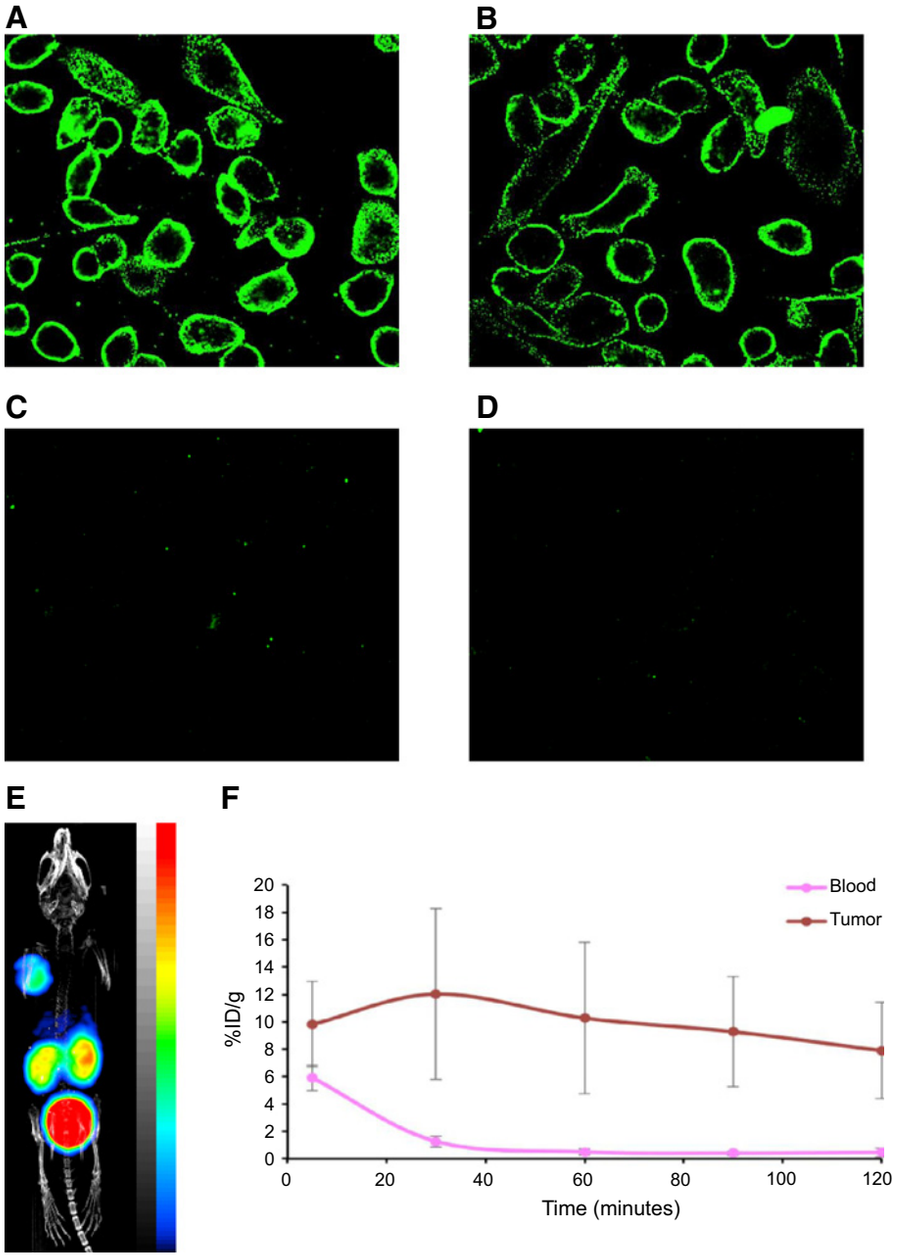

Figure 1.
HCS images showing anti-MMAE mAb staining (green) following test compound incubation with HT1080 cells: **A,** BT5528 (1 μmol/L); **B,** 1C1-MCMMAF (1 μmol/L); **C,** nonbinder BTC BCY6079 (3 μmol/L); **D,** MMAE (3 μmol/L); **E,** combined micro-PET/CT image showing Ga-68 radiolabeled BCY6099 exhibits high and specific tumor targeting (max 12 ± 6.3% ID/g, 30 minutes postdose), low uptake in nontarget tissues and rapid renal clearance. **F,** Quantification of radiolabeled *Bicycle* binder in tumor and blood.

Figure 4A illustrates growth curves in the PC3 model for BT5528 and BCY8245, an EphA2 nonbinder, (Supplementary Information T1). BT5528 gives rise to 80% tumor regression following every week intravenous dosing at 0.5 mg/kg. In contrast, at the same dose BCY8245 exhibits antitumor activity that is statistically different from vehicle responses but fails to achieve either tumor regression or tumor stasis. At the lower dose (0.167 mg/kg every week), BT5528 gives rise to 30% inhibition of tumor growth whereas at the same dose there is no difference in tumor growth between the vehicle and BCY8245-treated animals. The (limited) antitumor activity of BCY8245 is not surprising considering its cleavable VC linker and low molecular weight. BCY8245 rapidly distributes to tissues, including tumor tissue, where we expect to see payload release mediated by extracellular proteases in the tumor microenvironment. Similar observations have been made with nontargeting ADCs in preclinical studies. For example, nonbinder control ADCs delivering MMAE payload via a Val-Cit linker exhibit significant tumor growth reduction in the human tissue factor (TF) positive BxPC-3 xenograft model (albeit with less efficacy than the TF targeted ADC; ref. 36).

A key feature of our approach is to deliver a cell penetrant toxin (MMAE) following linker cleavage in the tumor microenvironment. We therefore used the PC3 model to make a pairwise comparison between BT5528, delivering the cell penetrant toxin MMAE and BCY10188, which delivers the noncell penetrant toxin MMAF. **Figure 4B** shows the effect of replacing MMAE with the noncell penetrant toxin MMAF. At all efficacious doses (0.33, 1.0, and 3.0 mg/kg every week), BT5528 gives rise to greater tumor growth inhibition than BCY10188, presumably because MMAE, but not

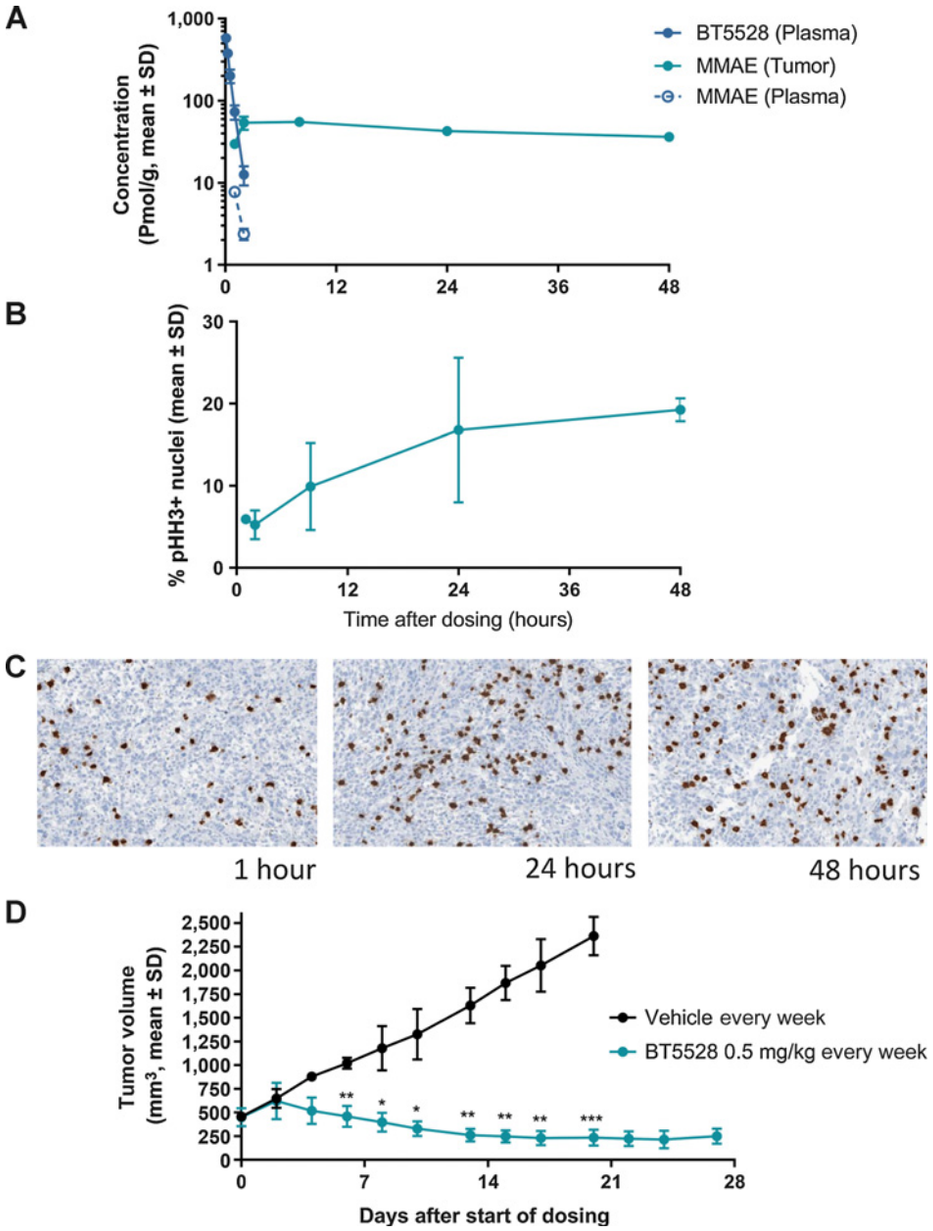

Figure 2.

BT5528 intravenous dosing at 0.5 mg/kg gives rise to transient MMAE levels in plasma and persistent exposure in tumor samples, efficacy in the PC3 xenograft model, and increased mitotic activity measured by PHH3 IHC staining. **A,** PK profiles of BT5528 and MMAE in plasma and MMAE in tumor samples following dosing with BB5528. Error bars indicate SD of $n = 3$. **B,** BT5528 gives rise to significant antitumor activity in the PC3 model following 0.5 mg/kg weekly dosing. Error bars indicate SD of $n = 3$ (*, $P < 0.05$; **, $P < 0.01$; ***, $P < 0.001$; two-way ANOVA with Sidak's multiple comparisons test). **C,** IHC pHH3 staining in tumor sections following intravenous dosing of BT5528 at 0.5 mg/kg. **D,** pHH3+ quantification in tumor sections following intravenous dosing of BT5528 at 0.5 mg/kg. Error bars indicate SD of $n = 3$

MMAF, gives rise to bystander activity in the tumor microenvironment. There are two potential mechanism of BT5528 bystander activity: extracellular linker cleavage and toxin penetration into neighboring cells, or receptor internalization and intracellular linker cleavage followed by release of cell penetrant toxin from lysed cells. The available data do not allow us to distinguish between these two mechanisms and it seems likely that BT5528 activity is mediated by toxin release following a combination of intracellular and extracellular linker cleavage.

We also explored the effect of replacing the cleavable Val-Cit linker with a noncleavable linker in the HT1080 model (**Fig. 4C**). As expected, BCY6063 is completely ineffective at a dose (10 mg/kg twice a week) 20-fold higher than a dose (3.0 mg/kg every week) achieving complete regression by day 7 in the same model (**Fig. 4C**; Supplementary Fig. S2).

To compare ADC and BTC targeting strategies, we explored the effect of BT5528 and 1C1-mcMMAF in preclinical xenograft models. MEDI-547 gives rise to excellent activity in the PC3 model (29). Our results (using 1C1-mcMMAF) replicated published results with MEDI-547 (18, 29) and showed that ADC and BTC delivery modalities are equipotent following comparable microtubule inhibitor doses: 1C1-mcMMAF 3.0 mg/kg every week; MMAF 0.06 mg/kg; BT5528 0.5 mg/kg every week, MMAE 0.08 mg/kg (**Fig. 5A**). The quoted mg/kg figures are calculated after taking into account the BT5528 1:1 toxin:*Bicycle* ratio and 1C1-mcMMAF 4:1 toxin:antibody ratio.

Conceptual models and experimental data support the hypothesis that low molecular weight peptide conjugates (molecular weight 4.4 kDa) achieve faster and greater tumor penetration and thus greater efficacy than antibody conjugates (molecular weight ~150 kDa). We

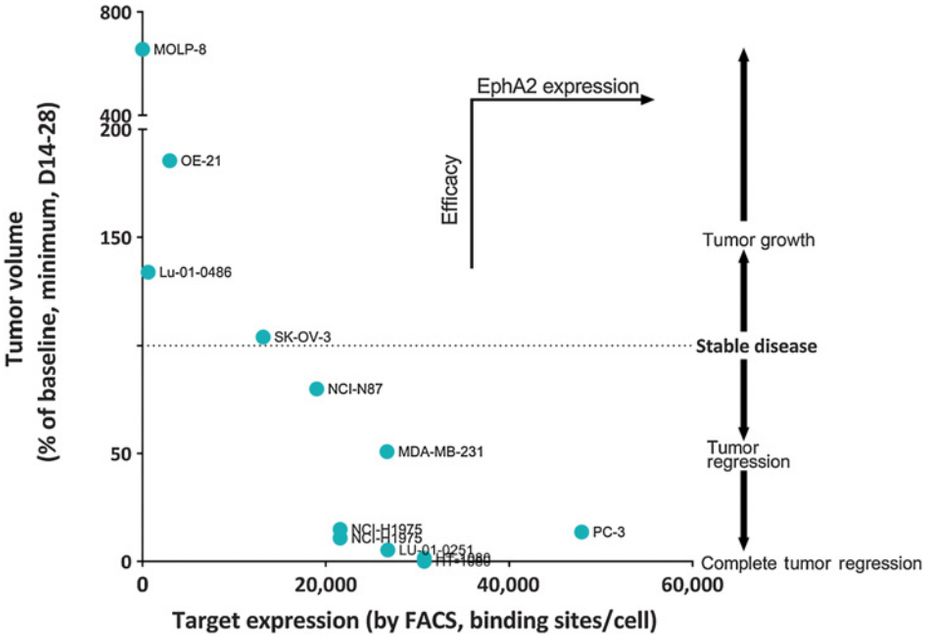

Figure 3.
EphA2 expression and tumor growth inhibition in CDX and PDX xenograft models are correlated. Y-axis: tumor volumes (expressed as percentage of D0 volume on D14-28). X-axis: EphA2 expression in CDX and PDX cell lines (EphA2 receptor counts per cell, measured by FACS).

would expect this effect to be more pronounced in large, poorly vascularized, tumors. We therefore tested BT5528 and 1C1-mcMMAF in small and large NSCLC PDX models. **Figure 5C** shows that BTC and ADC delivery give rise to broadly equivalent tumor regression in small NSCLC PDX tumors but BT5528 is much more effective than 1C1-mcMMAF in combating the growth of large NSCLC PDX tumors.

After demonstrating antitumor activity in large tumors, we wanted to determine if BT5528 has activity in a small tumor metastatic setting. To do this we modeled disseminated disease using intracardiac implantation of PC3 xenografts in mice and monitored growth of bone metastatic lesions by bioluminescence imaging. We initiated BT5528 treatment at two timepoints to capture the inhibitory effect with different tumor burden levels (15-fold difference in total tumor burden) and measured tumor burden over three or four cycles of weekly BT5528 dosing. When treatment was initiated with total tumor burden around 0.8×10^7 ph/seconds, we observed stasis over the 4-week treatment cycle (**Fig. 5C**). In contrast, when BT5528 treatment was initiated in animals with a larger tumor burden (12×10^7 ph/seconds), we observed decreased tumor burden and return to baseline values after three dosing cycles (**Fig. 5C**). Vehicle-treated animals exhibited rapidly increased tumor burden throughout the study and all of the animals succumbed by the end of the 4-week treatment period. As expected, BT5528-treated animals exhibited significantly ($P \leq 0.0001$, Mantel–Cox test) improved survival compared with vehicle-treated control animals (**Fig. 5E**).

Safety

The toxicology profile of the EphA2 ADC MEDI-547 included bleeding and coagulation events in the rat, NHP, and human (30). Our preclinical toxicology studies were therefore designed to identify both actual and incipient bleeding and coagulation toxicity following repeat dosing in the rat and monkey. The MTD in the rat was defined as 4 mg/kg following weekly dosing at 1, 2, and 4 mg/kg dosing for 5 weeks. The MTD in cynomolgus monkeys was determined to be 1.5 mg/kg following 5 weekly doses of 0.75, 1.5, and 3.0 mg/kg. We observed no effect on coagulation parameters [activated partial thromboplastin time (APTT), prothrombin time (PT)] and no evidence of bleeding or hemorrhage based on clinical signs and comprehensive gross- and histo-pathology assessments at any doses (up to and exceeding the MTD) in the rat or monkey (**Fig. 6**).

In both rat and monkey toxicology studies dose-limiting toxicology arose from decreased erythrocyte and leucocyte counts, with neutropenia highlighted as the most noteworthy toxicologic finding. We also observed histopathologic changes in tissues with a high mitotic rate (e.g., bone marrow and lymphoid tissue). We attribute the observed toxicology to nonspecific (antigen independent) linker cleavage and toxin release in the systemic circulation. At doses up to and including the MTD, there were minimal effects on organ weight in both tox species and no significant macroscopic or microscopic findings in the kidney or bladder.

Discussion

mAbs targeting cancer antigens offer an attractive approach to delivering cytotoxic payloads to tumors without incurring unacceptable side effects in nontarget organs. However, antibodies have physico-chemical and ADME properties which limit their efficacy in patients. The high molecular weight reduces the rate and extent of drug transit from plasma to tumor and drives metabolism and excretion through the liver, gall bladder, and GI tract. The plateau-like PK profile and long *in vivo* half-life necessitates the use of protease resistant linkers which only release payload following internalization and degradation in the lysosomal compartment, limiting activity to cells expressing the target antigen. In consequence, notwithstanding some success in the clinic, ADCs have proved to be a safe but only modestly effective way of administering high potency cytotoxic drugs to patients.

Our results show that phage-derived peptides have physicochemical characteristics that overcome some of the limitations inherent in antibody-based payload delivery. High ($12 \pm 6.3\%$ ID/g) concentrations of *Bicycle* peptide were found in implanted HT1080 xenografts

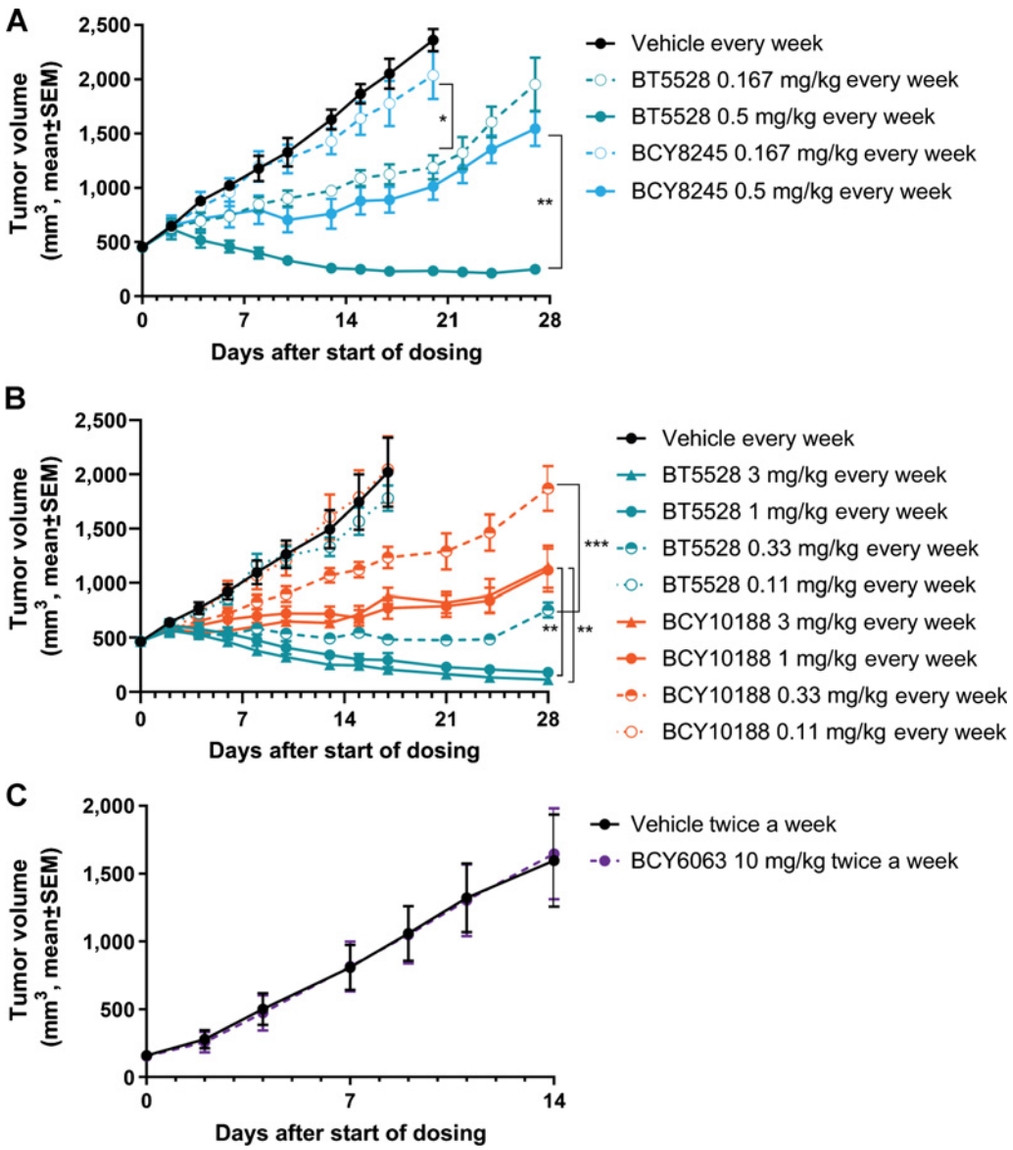

Figure 4.

BT5528 is efficacious in the PC3 xenograft model but control BTCs with noncleavable linkers and non-cell penetrant toxins lack comparable efficacy. **A,** The nonbinding BTC, BCY8245, is less active than BT5528 in the PC3 model (group mean ± SEM, $n = 5$) at both 0.5 and 0.0167 mg/kg dosing level (*, $P < 0.05$; **, $P < 0.01$; two-way ANOVA with Sidak's multiple comparisons test). **B,** Replacement of the cell penetrant toxin (MMAE: BT5528) with the non-cell penetrant toxin (MMAF: BCY10188) reduces activity in the PC3 model at 3, 1, and 0.33 mg/kg (group mean ± SEM; $n = 5$; *, $P < 0.05$; **, $P < 0.01$; two-way ANOVA with Sidak's multiple comparisons test). **C,** noncleavable linker chemistry abolishes activity in the HT1080 model; BCY6063, 10 mg/kg twice a week (group mean ± SEM, $n = 3$).

30 minutes after dose (**Fig. 1E**). This result is supported by bioanalysis of tumor and plasma samples, which showed that BT5528 releases MMAE payload in tumor and that released payload persists for long periods following disappearance of parent drug from plasma (**Fig. 1F**). *In vivo* xenograft experiments with cell permeable and cell impermeable auristatin analogues imply that BTC payload delivery gives rise to both direct and bystander cell killing (**Fig. 5B**).

PDX models are characterized by heterogeneous cell populations and differing levels of EphA2 expression. Consequently, agents that exclusively target high EphA2 expressing cells will fail to kill stromal and other cells with low levels of EphA2 expression. It is unclear if the superior efficacy we observed with BT5528 (compared with the EphA2 antibody conjugate) in a large tumor model (**Fig. 5C**) is mediated by improved tumor penetration, or increased bystander killing, or a combination of both effects.

A phase I study in patients with the EphA2 ADC MEDI-547 was discontinued when patients suffered adverse events, including liver, coagulation, and bleeding events at the starting dose (0.08 mg/kg (30)). No toxicologic findings were observed with animals administered 1C1 (anti-EphA2). Pharmacokinetic studies tracking parent conjugate

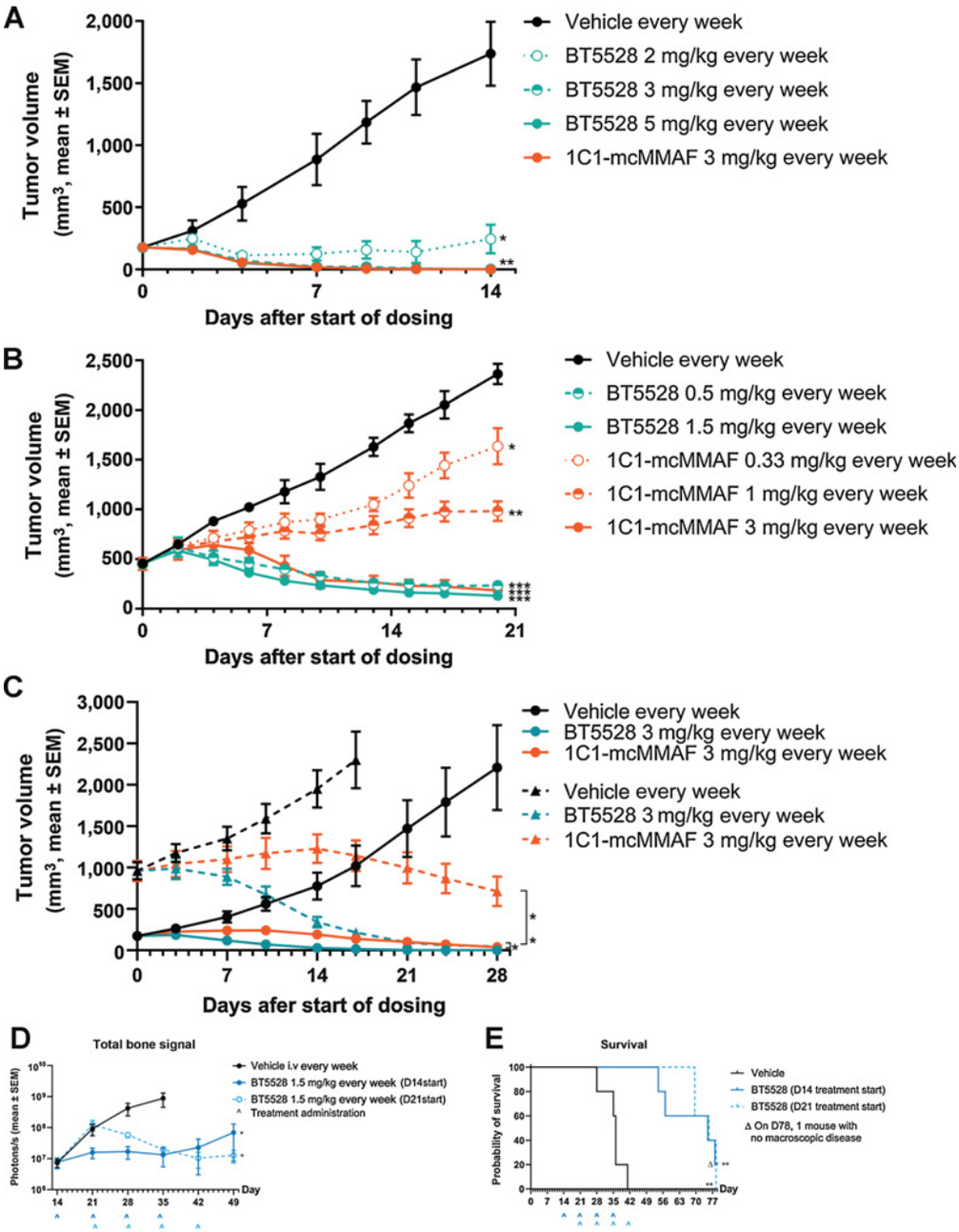

Figure 5.

A–C, BT5528 and the EphA2 ADC 1C1-mcMMAF give rise to comparable efficacy in HT1080, PC3, and NSCLC PDX models with low initial tumor burden (tumor volume < 300 mm^3); but BT5528 exhibits superior efficacy in the NSCLC model with high initial tumor burden (tumor volume ∼800 mm^3). **A,** BT5528 and 1C1-mcMMAF efficacy in the HT1080 model (group mean ± SEM; $n = 3$; *, $P < 0.05$; **, $P < 0.01$). **B,** BT5528 and 1C1-mcMMAF efficacy in the PC3 model (group mean ± SEM; $n = 5$; *, $P < 0.05$; **, $P < 0.01$). **C,** BT5528 and 1C1-mcMMAF efficacy in small (solid lines) and large (dashed lines) NSCLC (LU-01-0251) PDXs (group mean ± SEM; $n = 3$–6; *, $P < 0.05$; **, $P < 0.01$). Two-way ANOVA with Sidak's multiple comparisons test, compared with vehicle. **D–E**, BT5528 inhibits metastasis formation and prolongs survival in the PC3 metastasis model. **D**, BT5528 1.5 mg/kg every week treatment significantly reduces the total tumor cell burden (luciferase signal) in mandibles and femurs of mice with PC3 bone lesions (*, $P < 0.05$; mixed effects analysis from D14 to D35, $n = 5$). **E,** 4 weekly doses of 1.5 mg/kg BT5528 significantly increased the survival of mice with PC3 bone lesions (**, $P < 0.01$; Mantel–Cox log-rank test).

indicated that there was minimal or no dissociation of toxin from the EphA2 antibody and concentrations of cleaved MMAF metabolites were undetectable (30). The study authors therefore concluded that intact ADC and not released toxin was responsible for the observed toxicities (30). We observed no coagulopathy, DIC-like syndrome, or changes in closely monitored clotting parameters over the course of 5 weekly doses of BT5528 in toxicology studies in the rat and monkey (**Fig. 6**). These studies administered BT5528 doses, which on a mg/kg

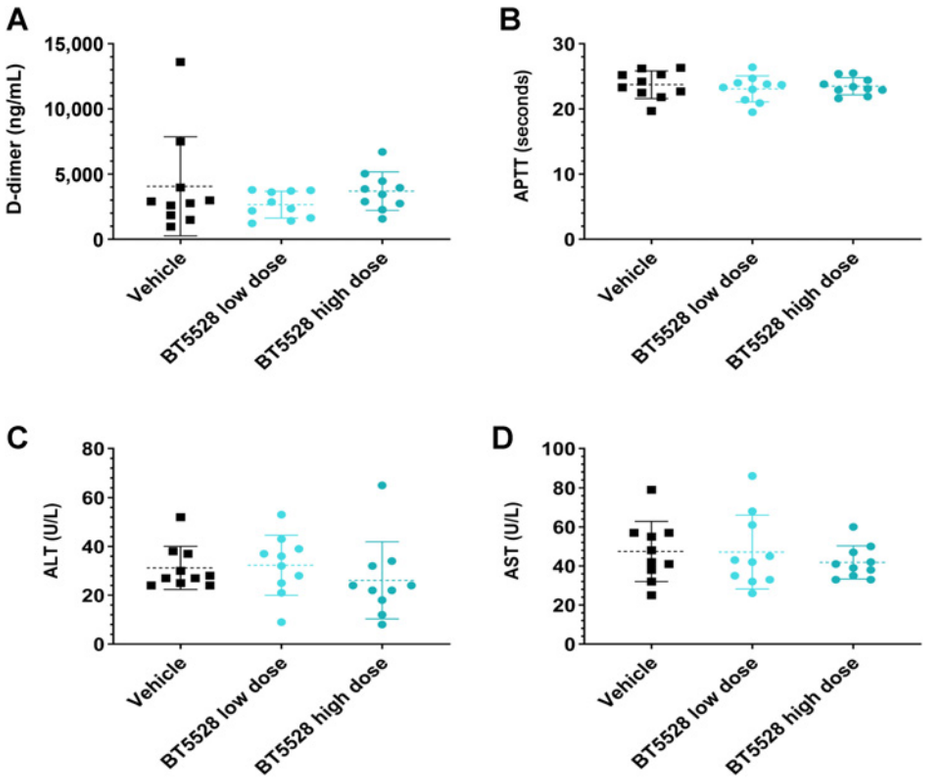

Figure 6.
BT5528 dosing to cynomolgus monkeys does not cause bleeding, coagulation, or liver toxicity: D-dimer, APTT, ALT, and AST responses (on day 32) following low (0.75 mg/kg) and high (1.5 mg/kg) BT5528 intravenous dosing to cynomolgus monkeys (three male and three female) on days 1, 8, 15, 22, and 29.

basis (and after standard allometric scaling) were eight and six times higher (in the rat and monkey, respectively) than the 0.08 mg/kg MEDI-547 dose that caused bleeding in patients after one or two doses (Supplementary Information T6). In terms of delivered payload, the BT5528 doses correspond to 53- and 39-fold more toxin payload (in the rat and monkey, respectively) than was delivered to patients using the EphA2 ADC (Supplementary Information T6). We attribute these contrasting toxicology responses to differences in the PK profiles of the intact BTC and ADC auristatin conjugates. Antibody payload delivery depends upon a plateau like PK profile that exposes target and nontarget organs to intact conjugate for days not hours. In contrast, BT5528 achieves prolonged toxin delivery to tumors, following transient exposure in plasma (**Fig. 2A**). Clinical testing in man is needed to discover if this PK profile gives rise to a favorable efficacy and toxicity trade-off in patients.

Taken together, these result supports the hypothesis that peptide-based payload delivery may overcome some of the drawbacks clinicians and drug discovery groups have encountered developing EphA2 ADC therapies and that BT5528 exhibits a preclinical profile that merits clinical evaluation in patients. A phase I trial in patients commenced in Q4 2019.

Disclosure of Potential Conflicts of Interest

G. Bennett is a Senior Director, Drug Development at Bicycle Therapeutics Ltd.; and has ownership interest (including patents) in Bicycle Therapeutics Ltd. A. Brown is a team leader at Bicycle Therapeutics Ltd.; and has Ownership Interest (including patents) in Bicycle Therapeutics Ltd. G. Mudd is a team leader. P. Huxley is a consultant at Bicycle Therapeutics Ltd. K. Van Rietschoten is a Team Leader - Peptide Chemistry at Bicycle Therapeutics Ltd.; and has ownership interest (including patents) in Bicycle Therapeutics Ltd. S. Pavan was a senior scientist at Bicycle Therapeutics Ltd.; and has ownership interest (including patents) in Bicycle Therapeutics Ltd. L. Chen is a Group Leader, Discovery at Bicycle Therapeutics Ltd.; and has ownership interest (including patents) in Bicycle Therapeutics Ltd. S. Watcham was a research scientist at Bicycle Therapeutics Ltd.; and has ownership interest (including patents) Stocks. Johanna Lahdenranta is a Director, in vivo Pharmacology at Bicycle Therapeutics Ltd. N. Keen is Chief Scientific Officer at Bicycle Therapeutics; and has ownership interest (including patents) in Bicycle Therapeutics Ltd. No potential conflicts of interest were disclosed by the other authors.

Authors' Contributions

Conception and design: G. Bennett, A. Brown, P. Huxley, K. Van Rietschoten, S. Pavan, L. Chen, J. Lahdenranta
Development of methodology: G. Bennett, A. Brown, K. Van Rietschoten
Acquisition of data (provided animals, acquired and managed patients, provided facilities, etc.): G. Bennett, G. Mudd, L. Chen, S. Watcham, J. Lahdenranta
Analysis and interpretation of data (e.g., statistical analysis, biostatistics, computational analysis): G. Bennett, A. Brown, G. Mudd, P. Huxley, S. Pavan, L. Chen, S. Watcham, J. Lahdenranta
Writing, review, and/or revision of the manuscript: G. Bennett, A. Brown, P. Huxley, L. Chen, S. Watcham, J. Lahdenranta
Administrative, technical, or material support (i.e., reporting or organizing data, constructing databases): G. Bennett, A. Brown, P. Huxley, S. Watcham
Study supervision: G. Bennett, A. Brown
Other (project leadership): P. Huxley, G. Bennett

Acknowledgments

This work was supported by Bicycle Therapeutics Ltd. The authors would like to acknowledge the contribution of Christina Annunziata & the Medimmune team for publishing results from the MEDI-547 clinical trial. Publication of the toxicities observed with MEDI-547 in clinical and preclinical studies greatly facilitated preclinical development and first in man testing of BT5528.

Received November 28, 2019; revised February 24, 2020; accepted April 29, 2020; published first May 12, 2020.

References

1. Biao-xue R, Xi-guang C, Shuan-ying Y, Wei L, Zong-juan M. EphA2-dependent molecular targeting therapy for malignant tumors. Curr Cancer Drug Targets 2011;11:1082–97.
2. Wang S, Placzek WJ, Stebbins JL, Mitra S, Noberini R, Koolpe M, et al. Novel targeted system to deliver chemotherapeutic drugs to EphA2-expressing cancer cells. J Med Chem 2012;55:2427–36.
3. Kamoun W S, Kirpotin DB, Huang ZR, Tipparaju SK, Noble CO, Hayes ME, et al. Antitumour activity and tolerability of an EphA2-targeted nanotherapeutic in multiple mouse models. Nat Biomed Eng 2019;3:264–80.
4. Godwin CD, Gale RP, Walter RB. Gemtuzumab ozogamicin in acute myeloid leukemia. Leukemia 2017;31:1855–68.
5. Bross PF, Beitz J, Chen G, Chen XH, Duffy E, Kieffer L, et al. Approval summary: gemtuzumab ozogamicin in relapsed acute myeloid leukemia. Clin Cancer Res 2001;7:1490–6.
6. Selby C., Yacko LR, Glode AE. Gemtuzumab ozogamicin: back again. J Adv Pract Oncol 2019;10:68–82.
7. Thurber GM, Dane Wittrup K. A mechanistic compartmental model for total antibody uptake in tumors. J Theor Biol 2012;314:57–68.
8. Li Z, Krippendorff BF, Sharma S, Walz AC, Lavé T, Shah DK. Influence of molecular size on tissue distribution of antibody fragments. mAbs 2016;8:113–9.
9. Lambert JM, Morris CQ. Antibody–drug conjugates (ADCs) for personalized treatment of solid tumors: a review. Adv Ther 2017;34:1015–35.
10. Park JE, Son AI, Zhou R. Roles of EphA2 in development and disease. Genes 2013;4:334–57.
11. Lindberg RA, Hunter T. cDNA cloning and characterization of eck, an epithelial cell receptor protein-tyrosine kinase in the eph/elk family of protein kinases. Mol Cell Biol 1990;10:6316–24.
12. Walker-Daniels J, Hess AR, Hendrix MJ, Kinch MS. Differential regulation of EphA2 in normal and malignant cells. Am J Pathol 2003;162:1037.
13. Abraham S, Knapp DW, Cheng L, Snyder PW, Mittal SK, Bangari DS, et al. Expression of EphA2 and Ephrin A-1 in carcinoma of the urinary bladder. Clin Cancer Res 2006;12:353–60.
14. Héroult M, Schaffner F, Augustin HG. Eph receptor and ephrin ligand-mediated interactions during angiogenesis and tumor progression. Exp Cell Res 2006;312:642–50.
15. Ireton RC, Chen J. EphA2 receptor tyrosine kinase as a promising target for cancer therapeutics. Curr Cancer Drug Targets 2005;5:149–57.
16. Kamat AA, Coffey D, Merritt WM, Nugent E, Urbauer D, Lin YG, et al. EphA2 overexpression is associated with lack of hormone receptor expression and poor outcome in endometrial cancer. Cancer 2009;115:2684–92.
17. Kinch MS, Moore M-B, Harpole DH. Predictive value of the EphA2 receptor tyrosine kinase in lung cancer recurrence and survival. Clin Cancer Res 2003;9:613–8.
18. Lee J-W, Stone RL, Lee SJ, Nam EJ, Roh JW, Nick AM, et al. EphA2 targeted chemotherapy using an antibody drug conjugate in endometrial carcinoma. Clin Cancer Res 2010;16:2562–70.
19. Lee J-W, Han HD, Shahzad MM, Kim SW, Mangala LS, Nick AM, et al. EphA2 immunoconjugate as molecularly targeted chemotherapy for ovarian carcinoma. J Natl Cancer Inst 2009;101:1193–205.
20. Saito T, Masuda N, Miyazaki T, Kanoh K, Suzuki H, Shimura T, et al. Expression of EphA2 and E-cadherin in colorectal cancer: correlation with cancer metastasis. Oncol Rep 2004;11:605–11.
21. Shao Z, Zhang W-F, Chen X-M, Shang Z-J. Expression of EphA2 and VEGF in squamous cell carcinoma of the tongue: correlation with the angiogenesis and clinical outcome. Oral Oncol 2008;44:1110–7.
22. Wang L-F, Fokas E, Bieker M, Rose F, Rexin P, Zhu Y, et al. Increased expression of EphA2 correlates with adverse outcome in primary and recurrent glioblastoma multiforme patients. Oncol Rep 2008;19:151–6.
23. Wykosky J. EphA2 as a novel molecular marker and target in glioblastoma multiforme. Mol Cancer Res 2005;3:541–51.
24. Yuan W-J, Ge J, Chen ZK, Wu SB, Shen H, Yang P, et al. Over-expression of EphA2 and EphrinA-1 in human gastric adenocarcinoma and its prognostic value for postoperative patients. Dig Dis Sci 2009;54:2410–7.
25. Han L, Dong Z, Qiao Y, Kristensen GB, Holm R, Nesland JM, et al. The clinical significance of EphA2 and Ephrin A-1 in epithelial ovarian carcinomas. Gynecol Oncol 2005;99:278–86.
26. Miyazaki T, Kato H, Fukuchi M, Nakajima M, Kuwano H. EphA2 overexpression correlates with poor prognosis in esophageal squamous cell carcinoma. Int J Cancer 2003;103:657–63.
27. Thaker PH, Deavers M, Celestino J, Thornton A, Fletcher MS, Landen CN, et al. EphA2 expression is associated with aggressive features in ovarian carcinoma. Clin Cancer Res 2004;10:5145–50.
28. Wu D, Suo Z, Kristensen GB, Li S, Troen G, Holm R, et al. Prognostic value of EphA2 and EphrinA-1 in squamous cell cervical carcinoma. Gynecol Oncol 2004;94:312–9.
29. Jackson D, Gooya J, Mao S, Kinneer K, Xu L, Camara M, et al. A Human antibody–drug conjugate targeting EphA2 inhibits tumor growth in vivo. Cancer Res 2008;68:9367–74.
30. Annunziata CM, Kohn EC, LoRusso P, Houston ND, Coleman RL, Buzoianu M, et al. Phase 1, open-label study of MEDI-547 in patients with relapsed or refractory solid tumors. Invest New Drugs 2013;31:77–84.
31. Heinis C, Rutherford T, Freund S, Winter G. Phage-encoded combinatorial chemical libraries based on bicyclic peptides. Nat Chem Biol 2009;5:502–7.
32. Mudd GE, Brown A, Chen L, van Rietschoten K, Watcham S, Teufel DP, et al. Identification and optimization of epha2-selective bicycles for delivery of cytotoxic payloads. J Med Chem 2020;63:4107–16.
33. Adams RH, Eichmann A. Axon guidance molecules in vascular patterning. Cold Spring Harb Perspect Biol 2010;2:a001875.
34. Kwan Tat S, Pelletier JP, Amiable N, Boileau C, Lajeunesse D, Duval N, et al. Activation of the receptor EphB4 by its specific ligand ephrin B2 in human osteoarthritic subchondral bone osteoblasts. Arthritis Rheum 2008;58:3820–30.
35. Dorywalska M, Dushin R, Moine L, Farias SE, Zhou D, Navaratnam T, et al. Molecular basis of valine-citrulline-PABC linker instability in site-specific ADCs and its mitigation by linker design. Mol Cancer Ther 2016;15:958–70.
36. Koga Y, Manabe S, Aihara Y, Sato R, Tsumura R, Iwafuji H, et al. Antitumor effect of antitissue factor antibody-MMAE conjugate in human pancreatic tumor xenografts. Int J Cancer 2015;137:1457–66.